Ocean Modelling 123 (2018) 98–109

Contents lists available at ScienceDirect

Ocean Modelling

journal homepage: www.elsevier.com/locate/ocemod

Understanding variability of the Southern Ocean overturning circulation in CORE-II models

S.M. Downes*[,a], P. Spence[b], A.M. Hogg[c]

[a] Antarctic Climate & Ecosystems Cooperative Research Centre, University of Tasmania, Hobart, Australia
[b] Climate Change Research Centre and ARC Centre of Excellence for Climate System Science, University of New South Wales, Sydney, Australia
[c] Research School of Earth Sciences and ARC Centre of Excellence for Climate System Science, Australian National University, Canberra, Australia

ARTICLE INFO

Keywords:
CORE-II models
Meridional overturning circulation
Southern Ocean
Eddy parameterisation
Ocean stratification
Water mass transformation

ABSTRACT

The current generation of climate models exhibit a large spread in the steady-state and projected Southern Ocean upper and lower overturning circulation, with mechanisms for deep ocean variability remaining less well understood. Here, common Southern Ocean metrics in twelve models from the Coordinated Ocean-ice Reference Experiment Phase II (CORE-II) are assessed over a 60 year period. Specifically, stratification, surface buoyancy fluxes, and eddies are linked to the magnitude of the strengthening trend in the upper overturning circulation, and a decreasing trend in the lower overturning circulation across the CORE-II models. The models evolve similarly in the upper 1 km and the deep ocean, with an almost equivalent poleward intensification trend in the Southern Hemisphere westerly winds. However, the models differ substantially in their eddy parameterisation and surface buoyancy fluxes. In general, models with a larger heat-driven water mass transformation where deep waters upwell at the surface (~ 55°S) transport warmer waters into intermediate depths, thus weakening the stratification in the upper 2 km. Models with a weak eddy induced overturning and a warm bias in the intermediate waters are more likely to exhibit larger increases in the upper overturning circulation, and more significant weakening of the lower overturning circulation. We find the opposite holds for a cool model bias in intermediate depths, combined with a more complex 3D eddy parameterisation that acts to reduce isopycnal slope. In summary, the Southern Ocean overturning circulation decadal trends in the coarse resolution CORE-II models are governed by biases in surface buoyancy fluxes and the ocean density field, and the configuration of the eddy parameterisation.

1. Introduction

Southern Ocean water masses are connected via the upper and lower meridional overturning circulation (MOC) cells, and the Antarctic Circumpolar Current (ACC). In a Southern Ocean zonal mean view, the upper cell of the MOC is driven by the upwelling of northern-sourced deep waters and northward surface Ekman transport (Speer et al., 2000). The lower MOC flows in the opposite direction, comprised of upwelled waters made denser by sea ice and mixing process along the Antarctic margin and of northward Southern Ocean abyssal flows. The strength of the ACC is linked to both the upper ocean meridional density gradient across it and the wind stress imparted upon the ocean surface (Russell et al., 2006; Boning et al., 2008; Meijers et al., 2012; Rintoul and Naveira Garabato, 2013; Farneti et al., 2015). The ACC transport and the residual (or total) transport of the upper MOC cell are generally thought to be enhanced by the poleward shift and intensification of the Southern Hemisphere westerlies (Morrison and Hogg, 2013; Farneti et al., 2010; Gent and Danabasoglu, 2011; Sijp and England, 2009; Saenko et al., 2012; Hogg et al., 2017). Eddies also play a large role in counteracting the influence of winds, more so for the ACC than the MOC (Morrison and Hogg, 2013). However, spatially and temporally biased observations, and modelling capabilities and parameterisations, inhibit our understanding of the long term variability of these circulation systems.

Multi-model analyses have been used for over a decade to elucidate major long term trends in the Earth's climate system. Whilst the mean across multi-model studies is often in good agreement with observations in variables such as winds, surface temperature and radiative fluxes, and precipitation (Gleckler et al., 2008), the inter-model spread is vast. Sparse spatiotemporal observational data can contribute to model spread in circulation magnitudes. For example, Farneti et al. (2015) showed that the transport of the upper MOC across models is in far better agreement with observationally-based estimates than the lower MOC, likely due to a denser distribution of

* Corresponding author.
E-mail address: s.downes@utas.edu.au (S.M. Downes).

https://doi.org/10.1016/j.ocemod.2018.01.005
Received 21 July 2017; Received in revised form 23 January 2018; Accepted 27 January 2018
Available online 31 January 2018
1463-5003/

observational data available within the upper 2 km of the ocean used to support model constraints.

The Southern Ocean overturning circulation upper and lower branches are connected by the incoming deep waters that upwell within the ACC region, and transport temperature anomalies and the oceanic response of climate forcing on decadal to centennial timescales (Armour et al., 2016). However, multi-model efforts, such as the Coordinated Ocean-Ice Reference Experiments Phase II (CORE-II; Danabasoglu et al., 2014), have revealed major differences and biases in the atmospheric and oceanic dynamics contributing to the meridional overturning circulation that limit our understanding of the temporally evolving climate system. For example, whilst the mean ACC transport in CORE-II models (150.3 ± 42.7 Sv, where 1 Sv equates to 10^6 m^3 s^{-1}; Farneti et al., 2015) agrees well with the long standing observational estimates (approximately 135 Sv Cunningham et al., 2003; Chidichimo et al., 2014), the model spread is around 50 Sv. Further, the most recent observational estimate for ACC transport is 175 Sv (Donohue et al., 2016), providing a new target for models to attain. Biases in sea ice (that contribute to the freshwater fluxes for Antarctic Bottom Water formation) remain poorly understood, with models failing to capture the sign and magnitude of Antarctic trends (Mahlstein et al., 2013; Downes et al., 2015; Shu et al., 2015). This study offers a new insight into the spread in overturning circulation across CORE-II climate models for the mean and varied states.

The CORE-II effort is comprised of coupled ocean-sea ice models forced by a common atmospheric state for the 1948–2007 period (Large and Yeager, 2009). The coherent atmospheric state (converted to surface fluxes using bulk formulae) is particularly advantageous in that influences of large-scale circulation, such as wind stress, are very similar across the CORE-II models. For example, the Southern Hemisphere westerly wind stress differs by no more than 10% in strength and less than 1° in latitude in position (Farneti et al., 2015). Yet the ocean circulation differs across the CORE-II models, due principally to model dynamics. The coupling of the CORE-II surface fields of wind speed, humidity, surface air temperature, and radiative fluxes to the ocean and sea ice models leads to a large spread in the magnitude of the variability in large scale circulation.

Downes et al. (2015) assessed the twelve CORE-II models presented here and found that the latitudinal position whereby the mid-latitude heat gain switched to high-latitude heat loss varied by more than 10°, and Farneti et al. (2015) showed a similar result for the decadal trend in surface heat fluxes. The mean state surface heat flux distribution contributes to the mid-latitude deep winter mixed layers, which varied by more than 150 m across the CORE-II models, and directly influences the rate of subduction of upper ocean water masses (Downes et al., 2015). In addition there were significant differences in the ocean temperature and salinity biases, the pattern of Weddell Sea deep convection, and the sea ice extent that all contribute to the lower overturning circulation and the formation of Antarctic Bottom Water. Farneti et al. (2015) found that the eddy-induced overturning circulation ranged by more than ± 6 Sv (more than half the magnitude of the model mean) across 17 CORE-II models due to the differing parameterisation of the eddy mixing scheme, with a 4.8 to 18.2 Sv range in the associated total upper branch of the MOC.

Downes et al. (2015) and Farneti et al. (2015) conducted extensive analyses on Southern Ocean water mass, sea ice and large-scale circulation processes in the CORE-II models, focusing particularly on the 1988–2007 period. Here we expand upon these analyses by evaluating the inter-model differences and biases that lead to the large spread in overturning circulation trends over the 1948–2007 period. Wind stress and buoyancy are known drivers of the ocean's large-scale circulation. The very similar trend in wind stress strength and position across the CORE-II models (Farneti et al., 2015) provides an opportunity to focus on the surface buoyancy and interior density model fields as mechanisms for changes in overturning circulation. However, we must also consider the eddy contribution to changes, given that each model employs its own version of an eddy advection scheme which can drastically affect the model response to surface forcings (Gent and Danabasoglu, 2011; Farneti et al., 2015).

This is the first study, to our knowledge, that associates decadal upper and lower overturning circulation trends with model biases in density and stratification, and eddy parameterisation configuration. In Section 2 we briefly outline model features of the twelve CORE-II models assessed, and the common metrics we use in this study. We describe the mean and temporal evolution of the upper and lower MOC, and its association with model buoyancy and density biases in Section 3, including an analysis of the relationship between the MOC, density and the westerly wind stress. We summarise and discuss our findings in Section 4.

2. Models and methods

2.1. The CORE-II models

We use 12 models from the CORE-II effort that are described in Danabasoglu et al. (2014), Downes et al. (2015) and Farneti et al. (2015), namely ACCESS, AWI, BERGEN, CMCC, GOLD, ICTP, KIEL05, MOM, MOM025, MRI, NCAR, and NOCS. The 12 models' features are detailed in Table 1, and we provide a brief overview here. Almost all of the models have a coarse resolution grid with approximately 1° horizontal spacing; exceptions are the MOM025 and KIEL05 models that have a 1/4° and 1/2° horizontal grid, respectively, and ICTP has a 2° horizontal resolution. The models have between 30 and 75 vertical levels. Mesoscale circulation is parameterised using a 1, 2 or 3-dimensional eddy diffusivity coefficient (Table 1) based on the Gent and McWilliams (1990) scheme that impacts the strength of the eddy induced overturning circulation and the extent to which the eddy overturning compensates variability in the Eulerian mean circulation. Note that the eddy-permitting MOM025 model does not use an eddy parameterisation. All the models are coupled to a sea ice model.

The inter-annually varying atmospheric state used in the twelve CORE-II models (Large and Yeager, 2009) provides common atmospheric surface temperature, wind speed, humidity and radiative fluxes for 1948–2007. The CORE-II models are simulated for 300 years (five 60-year CORE-forced cycles), and we assess the final cycle here. Trends in large-scale transports have been shown to remain consistent across each the 60-year cycles (e.g., see Fig. 22 in Farneti et al., 2015). We note that our conclusions for at least the upper overturning circulation hold regardless of whether we use the full 60 year CORE-II output or whether we disregard the first decade (after which the model has equilibrated to the new cycle). Using periods less than 50 years are not

Table 1
Details of the sixteen CORE-II and CMIP5 models used in this study. Table entries are taken from Danabasoglu et al. (2014), Farneti et al. (2015), and Downes et al. (2015). Shown are the model name used in this study, the ocean component, the horizontal grid resolution ($x \times y$), the vertical coordinate type and number of levels in parentheses, and the space-time characteristics of the eddy-induced advection coefficient. For the vertical coordinate, z is the geopotential coordinate, z* is the geopotential coordinate incorporating surface undulations, and σ_2 uses an isopycnal coordinate.

Model	Ocean	$x \times y$	z (No. levels)	Eddy scheme
ACCESS	MOM4p1	1° × (1/3-1)°	z* (50)	2D; time-dependent
AWI	FESOM	1° × (1/3-1)°	z (46)	3D; time-dependent
BERGEN	MICOM	1° × (1/4-1)°	σ_2 (53)	3D; time-dependent
CMCC	NEMO 3.3	1° × (1/3-1)°	z (46)	2D; time-dependent
GOLD	GOLD	1° × (1/3-1)°	σ_2 (63)	2D; time dependent
ICTP	MOM4p1	2° × (1-2)°	z* (30)	2D; time-dependent
KIEL05	NEMO 3.1.1	1/2° × 1/2°	z (46)	2D; time-dependent
MOM	MOM4p1	1° × (1/3-1)°	z* (50)	2D; time-dependent
MOM025	MOM5	1/4° × 1/4°	z* (50)	–
MRI	MRI.COM3	1° × 1/2°	z (50)	1D; fixed
NCAR	POP2	1° × (0.27-1)°	z (60)	3D; time-dependent
NOCS	NEMO 3.4	1° × (1/3-1)°	z (75)	2D; time-dependent

ideal for distinguishing models with a smaller or larger magnitude in the MOC decadal trends.

For ocean interior variables, we compare the CORE-II models to two versions of the World Ocean Atlas (WOA) climatologies, WOA09 (Locarnini et al., 2010; Antonov et al., 2010) and WOA13 (version 2 Locarnini et al., 2013; Zweng et al., 2013). The former has been produced on a 1° grid with 33 vertical levels, whilst the WOA13 climatology includes an additional decade of climatology data compared to WOA09, and is available on a 1/4° grid with 102 vertical levels.

2.2. Definitions and Calculations

In this study the MOC is defined as the zonal integration and vertical cumulative sum (in depth or density space) of the meridional velocity. The upper and lower overturning circulation here is the combination of the eddy induced and Eulerian mean circulations, known as the residual or total circulation. Trends and changes in the MOC cell strengths used throughout the study are based on calculations using absolute values, that is, a positive trend will indicate increases and negative values for decreases. Our MOC results are presented in density coordinates (referenced to 2 km), with units in Sv. The MOC in the classic depth coordinate does not equate to the same as the more natural density coordinates (e.g., Döös and Webb, 1994), and future changes in the MOC in depth and density space differ in sign and magnitude (Downes and Hogg, 2013).

The upper cell in density coordinates (MOC_{UC}; clockwise directed; positively signed) is defined as the maximum strength in the density range, $1035 < \sigma_2 < 1036.5$ kg m^{-3}, between 60°S and 30°S. The lower cell in density coordinates (MOC_{LC}; counter-clockwise directed; negatively signed) is defined as the absolute maximum strength in the density range, $1036.5 < \sigma_2 < 1037.5$ kg m^{-3}, between 60°S and 30°S. We restrict the southern boundary of our MOC_{LC} definition at 60°S because we do not want to confuse its trend with that of the subpolar cell in the same density range.

The eddy-induced overturning circulation in density space, MOC_{GM}, has more than one maxima in the Southern Ocean in several models (Farneti et al., 2015; see their Fig. 18), thus we *average* the eddy contribution to the MOC across a range of densities. Farneti et al. (2015) showed that the time-mean averaged MOC_{GM} was associated with the eddy induced advection coefficient used in the eddy parametrisation scheme (see their Fig. 21). We follow the definition used in Farneti et al. (2015) where the MOC_{GM} is averaged over the density range $1034.5 < \sigma_2 < 1037.5$ kg m^{-3} and latitude range of 70°S–35°S. Note that the MOC_{GM} flows in the same direction as the MOC_{LC}, and flows across both the lower and upper MOC density ranges (Saenko et al., 2012). The MOM025 model excludes an eddy parameterisation and the GOLD model did not archive the eddy contribution; these models are highlighted by an asterisk in figures where we illustrate MOC_{GM} diagnostics.

Given that the CORE-II models are coupled to a common atmospheric state, we pay particular focus to the surface and interior density-related properties that may alter the large-scale circulation. We use the surface water mass transformation (WMT) diagnostics estimated in Downes et al. (2015, see their Figs. 14 and 15), and first introduced in Walin (1982), to show how atmosphere-ocean surface buoyancy fluxes of heat and freshwater combine to alter the surface density. The surface transformation is an integration over the entire water mass outcrop region (bounded by ρ_k and ρ_{k+1}, where $\rho_{k+1} > \rho_k$), and is estimated as (following Downes et al., 2011; 2015):

$$F(\rho_k) = -\frac{1}{(\rho_{k+1} - \rho_k)} \iint_A \left\{ \frac{\alpha Q_{net}}{C_p} \right\} dA + \frac{1}{(\rho_{k+1} - \rho_k)} \iint_A \{\rho_0 \beta S (FW_{net})\} dA. \quad (1)$$

There are two main terms in the surface water mass transformation estimate. The first represents the transformation due to the net heat flux into the ocean (Q_{net}) and its associated thermal expansion and heat capacity coefficients (α and C_p, respectively). The second term represents the net freshwater flux into the ocean (FW_{net}), including precipitation, evaporation, run-off and sea ice melt, and associated haline contraction coefficient (β), surface salinity (S), and reference ocean density (taken here to be $\rho_0 = 1035$ kg m^{-3}). Positive transformation rates indicate where lighter water masses are converted to denser layers associated with surface buoyancy loss, and negative rates with conversion to lower densities due to surface buoyancy gain.

3. Results

3.1. The mean state of the MOC

We begin by describing the mean state of the density, wind stress and overturning circulation to help orient the reader, and then link these mean states to decadal variability in the MOC. All density and overturning circulation diagnostics are calculated online and archived as monthly means. The zonal mean ocean density is very similar for the upper kilometre of the ocean in the CORE-II models (Downes et al., 2015), given that the models are forced by the same atmospheric state. By the end of the 60 year CORE-II analysis period, the isopycnals have deepened in the Southern Ocean interior north of 60°S, consistent with warming and freshening trends, and shoal south of 60°S (Fig. 1a). The strong westerly winds, that steepen isopycnals and act to strengthen the Eulerian upper overturning circulation, increase by approximately 30% in its maximum strength and shift poleward by 3° to around 54° latitude by 2007 (Fig. 1b; see also Fig. 2 in Farneti et al., 2015).

3.1.1. The upper and eddy-induced overturning cells

The Southern Ocean MOC in density space is comprised of an upper cell in the 60°–30°S latitude range and, at higher densities, the lower cell, flowing in the opposite direction (Fig. 2; c.f. Farneti et al., 2015). The residual MOC is comprised of the Eulerian and eddy-induced circulation, the latter being distributed in density space across both the upper and lower overturning cells. The maximum strength of the net upper and lower MOC, and the average eddy-induced MOC, over the Southern Ocean are illustrated in Fig. 3. The CORE-II model mean (that is, the average of all twelve models) is in good agreement with observationally based MOC_{UC} estimates of approximately 12 Sv (Lumpkin and Speer, 2007), with considerable spread across the individual models (Fig. 3a). Models with a larger MOC_{UC} are those with the upper cell extending across larger density ranges and latitudes, specifically the ACCESS, AWI, CMCC, KIEL, MOM, MOM025 and MRI models (see where the upper cell extends south of 60°S in these models in Fig. 2).

Farneti et al. (2015) showed that models with a more complex, three-dimensional eddy parameterisation (AWI, BERGEN, and NCAR) produced a larger eddy contribution to the MOC (red circles in Fig. 3b). However, among the models with a two-dimensional (depth independent) eddy parameterisation, several have a large range for the eddy advection coefficient that extends up to 5000 m^2 s^{-1} (CMCC, ICTP, KIEL05, and NOCS). This extended coefficient range also increases the magnitude of the eddy-induced overturning circulation. Conversely, a one-dimensional eddy parameterisation or two-dimensional eddy parametrisation with a smaller advection coefficient range (i.e., up to 1000 m^2 s^{-1}) produces a small eddy-induced overturning (blue circles in Fig. 3b).

3.1.2. The lower overturning cell

In climate models, the deep ocean is one of the most poorly represented ocean regions, primarily due to sparse observations, coarse model vertical grid resolution, and mesoscale parameterisations that are fixed or depth/time independent. The lower overturning circulation in density space (MOC_{LC}) varies considerably across climate models (Downes and Hogg, 2013; Farneti et al., 2015), linked to ocean temperature and salinity biases throughout the water column (Heuzé et al., 2013; Wang et al., 2011). Here, MOC_{LC} in the final 20 years of each

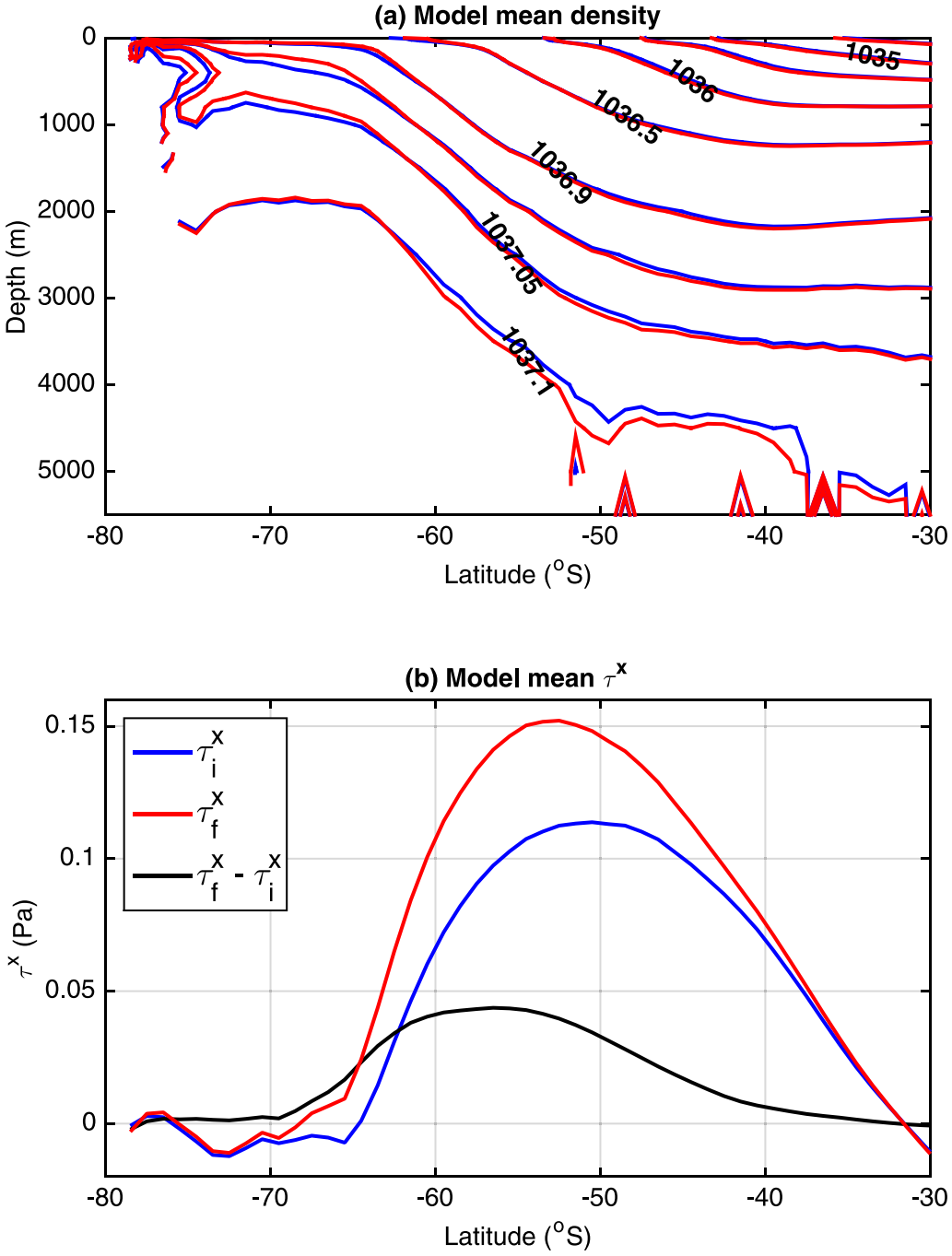

Fig. 1. Zonal mean density (σ_2; kg m^{-3}) for the first (blue) and last (red) 20 years, averaged across the twelve CORE-II ('Model mean') in the Southern Ocean. (b) Multi model mean zonal mean wind stress (Pa) for the first (τ_i^x; blue) and last (τ_f^x; red) 20 year averages for the CORE-II model mean, and the difference (τ_f^x–τ_i^x; black). Positive wind stress represents stress in the eastward direction. (For interpretation of the references to color in this figure legend, the reader is referred to the web version of this article.)

experiment varies from 5 Sv in the eddy permitting MOM025 model to 22 Sv in GOLD (Fig. 3c). Most of the MOC_{LC} estimates are lower than observationally-based estimates (16–29 Sv; Lumpkin and Speer, 2007; Talley, 2013). Models with weak MOC_{LC} can have a strong MOC_{UC} (e.g. Kiel05, MOM025 and MRI) and vice versa (e.g. BERGEN and GOLD and NOCS).

To the south of the lower MOC lies a subpolar cell that is driven by convection and sea ice variability (Fig. 2). We find that this subpolar cell is significantly correlated to the strength of the lower cell (MOC_{LC}) in eight of the twelve CORE-II models over the 60 year period (figure not shown). However, we were unable to find a distinct link between variability in polar seas and that in the lower MOC cell due to the large spread in convection rates and patterns. For example, the MOC_{LC} consistently decreases, but there is no consistent trend in the Weddell Sea mixed layer depth, an indicator of deep water formation. Thus the subpolar cell does not likely contribute to the decreasing trend in the MOC_{LC}, and we focus on understanding the coherent model trends in the lower and upper MOC between 30°S and 60°S.

3.2. Temporal variability of the MOC

3.2.1. The upper overturning cell

Here we examine decadal variability in the overturning circulation as a function of the model and varying surface buoyancy fluxes,

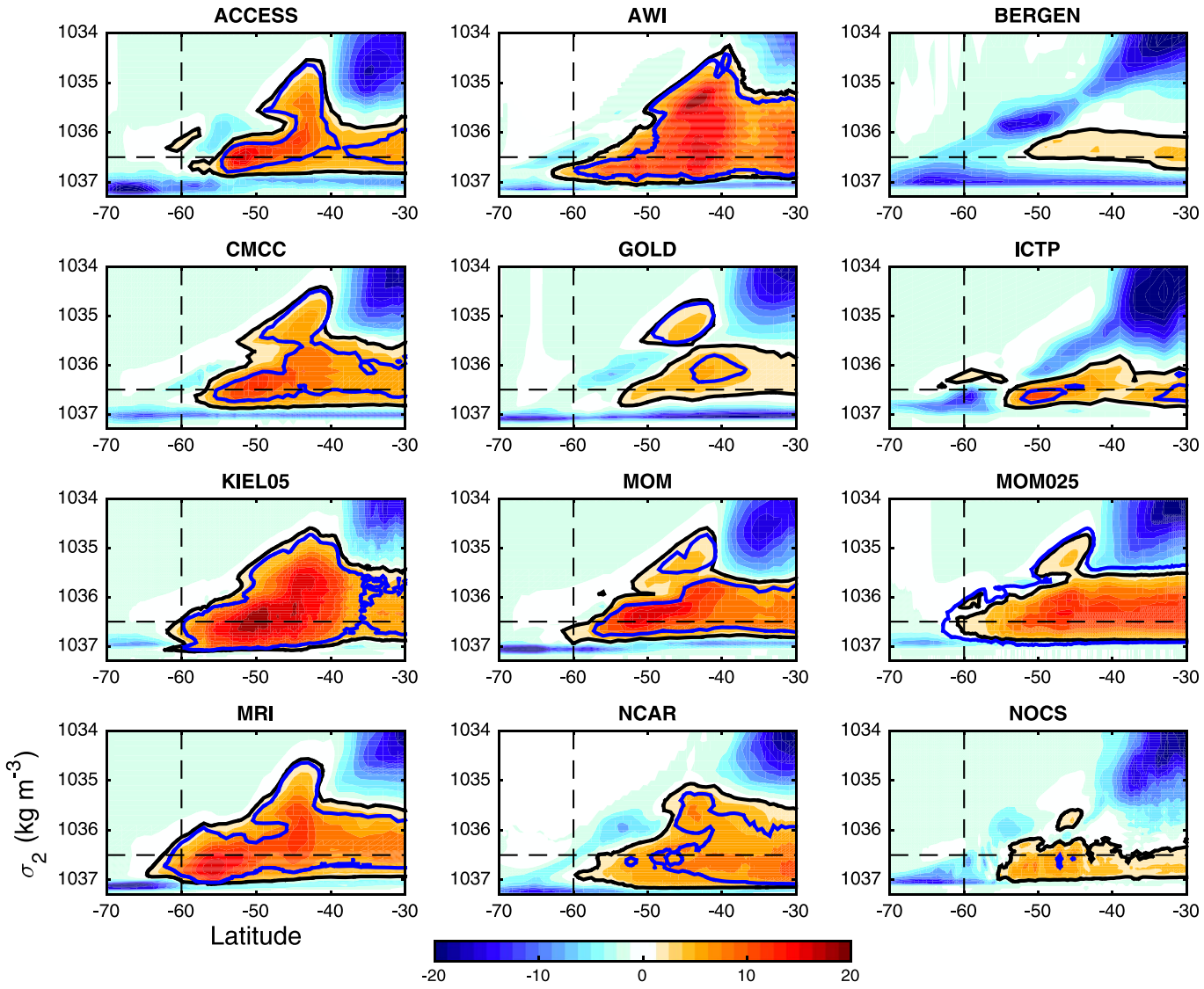

Fig. 2. Southern Ocean meridional overturning circulation (Sv) for the 60 year average (1948–2007). Positive (reds) indicate overturning in the clockwise direction; blues for counter-clockwise circulation. The blue and black contours represent the + 2 Sv contour for the first and last 20 years averages, respectively. The dashed lines show where the 1036.5 kg m^{-3} and 60°S intersect as a point of reference for describing the spatial distribution of the upper MOC.

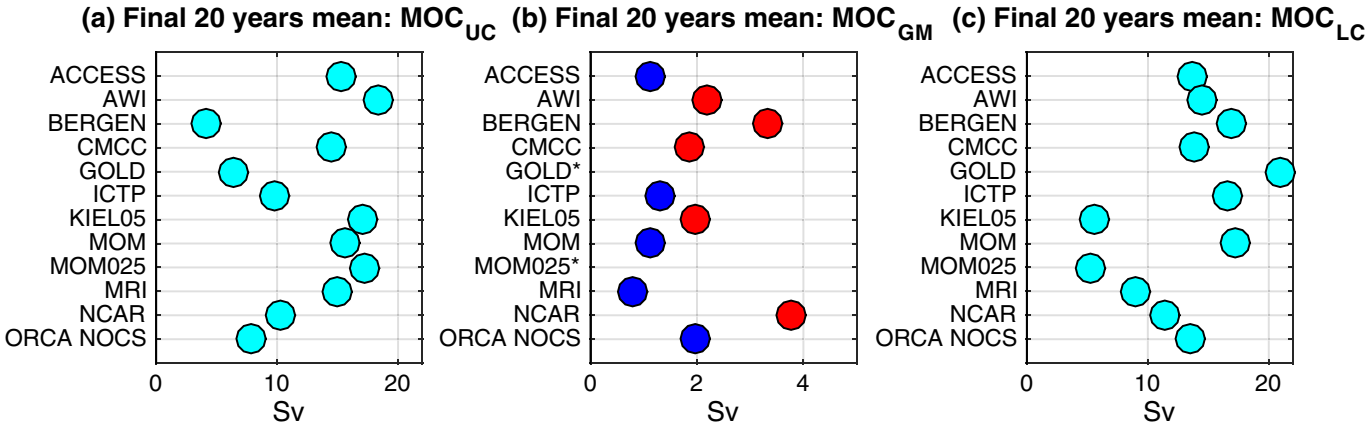

Fig. 3. The final 20 year mean (1988–2007) of the (a) MOC_{UC}, (b) MOC_{GM} and (c) MOC_{LC}. All transports are given as absolute values in units of Sv. In panel (b), the red/blue colours indicate the models that show weaker/stronger decadal MOC_{UC} trends in Fig. 4.

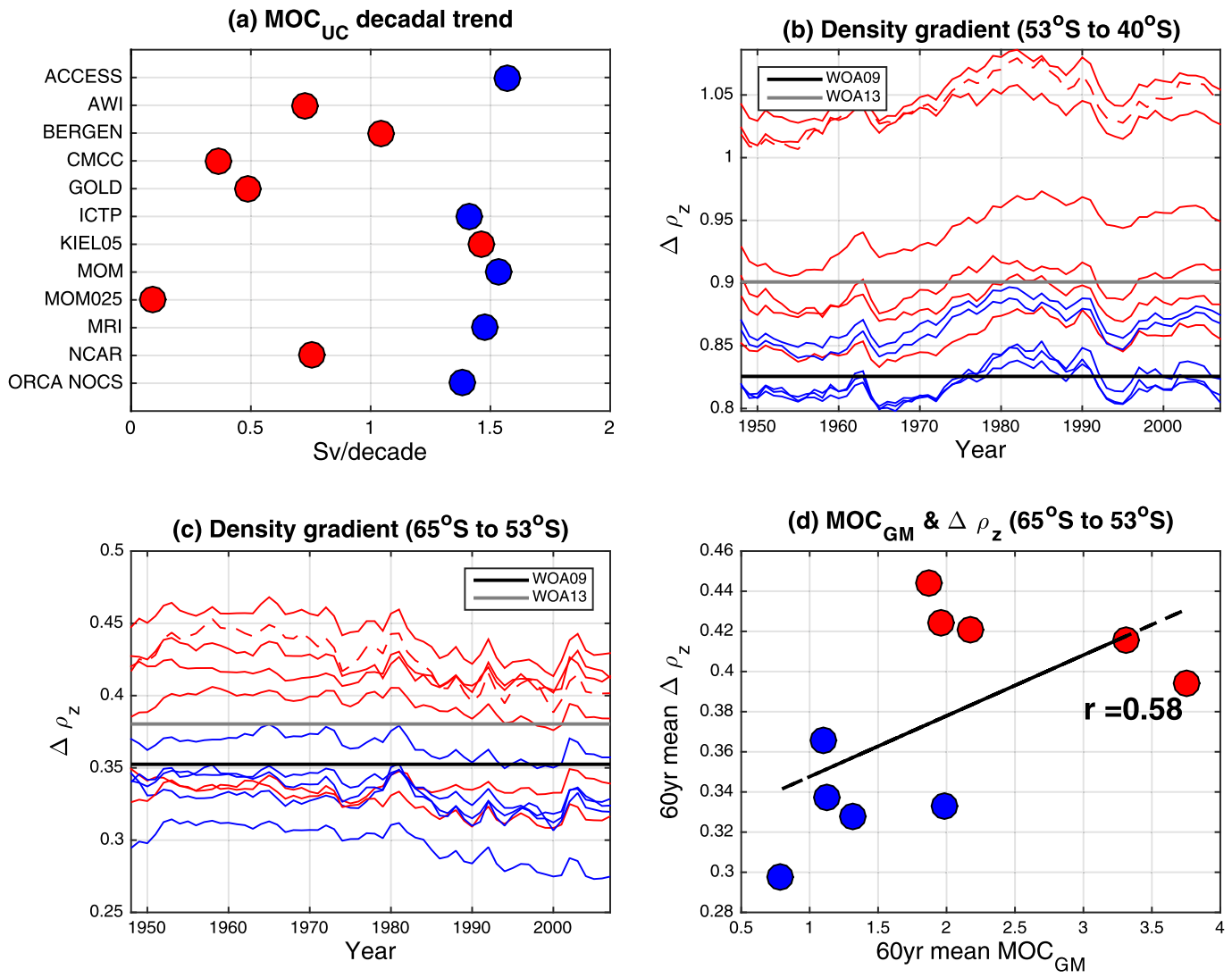

Fig. 4. (a) 60 year trend (Sv/decade) for the MOC_{UC} in each CORE-II model, where the models in red have a smaller trend and blue dots represent models with a larger trend. (b) The zonal mean vertical density gradient for the 53–40°S region (i.e. the region north of the approximate wind stress maximum), where the gradient ($\Delta\rho_z$) is defined as the zonally and vertically averaged density in the 1–2 km range minus that in the 0–1 km range. A positive gradient thus indicates that the 1–2 km density layer is denser than that above, with a larger gradient indicative of a larger difference and stronger stratification in the upper 2 km of the ocean. (c) Same as in panel (b), except averaged over the 65–53°S region (i.e. the region south of the approximate wind stress maximum). (d) The 60 year mean MOC_{GM} for each model versus the 60 year mean of the density gradient timeseries in panel (c), that is, south of the wind stress maximum in the ACC region. The black dashed curve is the line of best fit, with a correlation across ten models of 0.58 (significant at the 90% level). Note: GOLD and MOM025 are excluded in this correlation. In all panels, the models that have the largest temporal trend for MOC_{UC} are displayed in blue, and the smallest in red. In panels b and c, the red dashed curve is the KIEL05 model and BERGEN is an outlier, and the black/gray thick dashed curves represents observations from the World Ocean Atlas (WOA09/WOA13). (For interpretation of the references to color in this figure legend, the reader is referred to the web version of this article.)

stratification, and eddy parametrisation. We begin with the upper ocean density variability in the latitude range (60°–30°S) where the MOC_{UC} is defined. In the CORE-II models, the MOC_{UC} increases by 0.1 to 1.6 Sv/decade (Fig. 4a), with the lowest trends found in the AWI, CMCC, GOLD, MOM025 and NCAR models. In the mean state, these five models and KIEL05 have a stronger vertical density gradient north of the wind stress maximum that is evident across the 60 year CORE-II period (Fig. 4b and c). That is, the density difference between the 0–1 km and 1–2 km depth ranges is greater in these models, and thus the stratification is stronger. This stronger upper ocean stratification, maintained by surface warming and freshening (see Figs. 10–12 in Farneti et al., 2015), is associated with weak winter mixed layer trends in the same region (see Fig. 22 in Downes et al., 2015). We note that the density in the 0–1 km range is very similar across the models, thus it is the density in 1–2 km that dominates the density differences in Fig. 4b and c. The CORE-II models have a vertical density gradient that spans observational estimates from both the WOA09 and WOA13 climatologies.

It is interesting to note that the WOA13 observational climatology lies within the upper density gradient range of the models with a weak MOC_{UC} decadal trend (red), however the earlier WOA09 version lies within the range of models that exhibit a larger MOC_{UC} trend (blue). We also note some exceptions to the model results. The MOC_{UC} decadal trend in the KIEL05 model is large, despite this model having a higher vertical density gradient. Further, the BERGEN model has a MOC_{UC} decadal trend that is mid-range (~ 1 Sv/decade; Fig. 4), a smaller vertical density gradient, but a higher eddy induced overturning circulation (Fig. 3b).

The choice of eddy parameterisation influences upper ocean density by reducing the isopycnal slope and thus increasing the density

difference between the 0–1 km and 1–2 km depth ranges. We find that the models with a 3D eddy parameterisation (AWI, BERGEN and NCAR) are among the models with a smaller decadal *trend* in the MOC_{UC} of under 1.2 Sv/decade (mostly red circles in Fig. 4a). In contrast, models with a 1D or 2D eddy parameterisation (blue circles; e.g., ACCESS, ICTP, MOM, MRI and NOCS) tend to have a smaller eddy-induced overturning circulation (Fig. 3b), but a larger trend (Fig. 4a). Our upper MOC cell results are in agreement with previous studies that show the eddy-induced circulation reduces the influence of the poleward intensifying wind stress (Fig. 1b) on the residual MOC_{UC} (see also, for example, Saenko et al., 2012; Farneti et al., 2015; Gent, 2016; Chapman and Sallée, 2017; Marshall et al., 2017).

In Fig. 4d, we evaluate the relationship between the vertical density change in the upper 2 km in the ACC region and the average strength of the eddy-induced overturning circulation. Within the 65–53°S latitude range (south of the wind stress maximum; displayed in the Fig. 4d), we find a significant correlation between eddy-induced overturning and the upper ocean vertical density gradient ($r = 0.58$). Models with a weak MOC_{UC} decadal trend, including some of which have a more complex 3D eddy parameterisation (AWI, BERGEN and NCAR), have a larger density gradient, and vice versa for the larger MOC_{UC} trends. However, we do not find a strong correlation between the eddy-induced overturning circulation averaged over the CORE-II period and the vertical density gradient in the region north of the wind stress maximum ($r = 0.28$; 53°–40°S; figure not shown). Thus, the eddy overturning circulation is most influential in the upwelling region of the ACC.

3.2.2. The lower overturning cell

Whilst the MOC_{UC} increases coherently across the twelve models, the MOC_{LC} coherently decreases, consistent with recent deep ocean temperature, salinity and volume trends (Purkey and Johnson, 2012). The MOC_{LC} decreases by 0.5–1.7 Sv per decade across the twelve models (Fig. 5a), with the largest trend in the BERGEN, MOM025, MRI and NOCS models, followed by the ACCESS, AWI and ICTP models (close to 1 Sv/decade). We note that four of the six models with a weaker MOC_{LC} trend, namely CMCC, GOLD, KIEL05 and NCAR, also have a weaker MOC_{UC} trend, a stronger upper ocean density gradient (Fig. 4), and a more complex, three-dimensional (or no) eddy parameterisation (Fig. 3). Whilst the sign of the MOC_{LC} trend is coherent, the variations in magnitude can be understood by again looking at the ocean interior density properties. The MOC_{LC} is prominent at densities greater than 1036.9 kg m^{-3} (Fig. 2), which is in the depth range greater than 2 km for the regions approximately bound by 40°S and 40°N (Fig. 1a).

Spence et al. (2014) showed that changes in the MOC_{LC} due to wind stress variability can be attributed to the density components of the potential vorticity budget. Here, we estimate the potential vorticity (Fig. 5b and c), defined as $(f/\rho_0) \times (\delta\rho/\delta z)$, where f represents the Coriolis force, ρ_0 is the mean ocean density, and $\delta\rho/\delta z$ is the vertical change in the local density. For depths greater than 2 km, we find that the mean state potential vorticity is larger in models with a larger MOC_{LC} decreasing trend (black dots), and smaller for models with weaker MOC_{LC} decreasing trends. In short, a weaker deep ocean stratification, sustained over the 60 year CORE-II period, reduces the weakening of the lower overturning circulation. Further, the observational estimates for the present day climate (blue and cyan dashed lines in Fig. 5b) lie in the weakly stratified (low PV) values.

Despite a fairly coherent result regarding the MOC trends and density and stratification illustrated in Figs. 4 and 5, we do note some exceptions. The MOC_{LC} decadal trend in the ICTP model is large (-1.1 Sv/decade) even though this model shows a low potential vorticity. Conversely, the NOCS model, which falls clearly in the large MOC_{LC} category, also exhibits a cool 1–2 km temperature bias in the mean state. These discrepancies (as well as those in the BERGEN and KIEL05 models for the MOC_{UC} results) may be due to a number of reasons, such as sea ice variability, chosen vertical coordinates, grid resolution, and possible biases arising from averaging in our estimates.

The question remains as to how this stronger or weaker deep ocean stratification is developed and maintained. We find that temperature biases within the intermediate water mass layers (approximately 1 to 2 km) are reflected in the deep ocean potential vorticity. A warm bias in the mean state across mid to high latitudes (black curves; compared with observations) is found in models where the deep ocean stratification is stronger and the decreasing trend in the MOC_{LC} is larger in magnitude (Fig. 5d). Variations in temperature in the 1 to 2 km depth range also influences deep ocean stratification and the overturning circulation. There is a cool bias with temperature cooling (negative; Fig. 5d and e) across low- and mid-latitudes for the models with a weaker MOC_{LC} trend (magenta curves), and warm bias and warming for models with a larger MOC_{LC} decadal trend (black curves). Similarly, salinity has an increasing trend for models with a smaller MOC_{LC} decadal trend for the 1 to 2 km depth range, with little distinction across models for depths lower and higher than this range (figure not shown). Thus the cooling and increasing salinity trends in the 1 to 2 km range are associated with the stratification below 2 km over the 60 year CORE-II period.

3.2.3. Water mass transformation

Whilst eddies play a role in the upper ocean stratification in the 1 to 2 km depth range (Fig. 4d), we must also consider the formation processes at the ocean surface contributing to intermediate waters that are exported in this depth range. The surface heat and freshwater fluxes in the CORE-II models are influenced by the individual model surface temperature and salt and sea ice. Downes et al. (2015) showed that the zonal mean surface heat fluxes varied substantially in sign across Southern Ocean latitudes (see their Fig. 3). In Fig. 6, we illustrate the conversion of Southern Ocean water mass classes (south of 30°S) that results from monthly changes in the surface heat and freshwater flux input into the first model ocean layer. A negative water mass transformation (WMT) rate implies the water mass in a particular density class has a buoyancy gain in its outcrop density range and is transformed to a lighter density class.

Deep waters that upwell to the surface in the Southern Ocean (around 1035.5–1036.5 kg m^{-3}) are transformed into lighter intermediate waters via buoyancy gain. In particular, the models with a larger MOC_{LC} decadal trend (black dots; Fig. 5a) have a greater transformation rate from deep waters to lighter densities, due to surface heat fluxes (Fig. 6a and c). In short, the upwelled deep waters in these models are becoming warmer as they transform to intermediate waters. Thus, models with a larger decreasing MOC_{LC} trend also have warmer water subducted into their 1–2 km depth range (also shown in Fig. 5; lower panels) that strengthens deep ocean stratification. Further, the surface water mass transformation due to oceanic heat gain doubles by the end of the 60 year CORE-II period (compare panels a and c in Fig. 6). We did not find any distinct differences between the 'black' and 'magenta' models for the freshwater-based surface water mass transformation (Fig. 6b and d).

We also look at how these surface WMT terms change over the CORE-II period (Fig. 6e and f). We find that both heat and freshwater fluxes change similarly across the CORE-II models, and this temporal change is not associated with the magnitude of the MOC_{LC} decadal trends in Fig. 5a. Thus, it is the difference in the surface heat WMT contribution in the models in the mean state (and not its temporal evolution) that is associated with trends in the lower overturning circulation. Further, the largest heat and freshwater fluxes changes occur in the deep water density range ($1036 < \sigma_2 < 1037.1$ kg m^{-3}; Fig. 6e and f), which corresponds with the density range where we find the

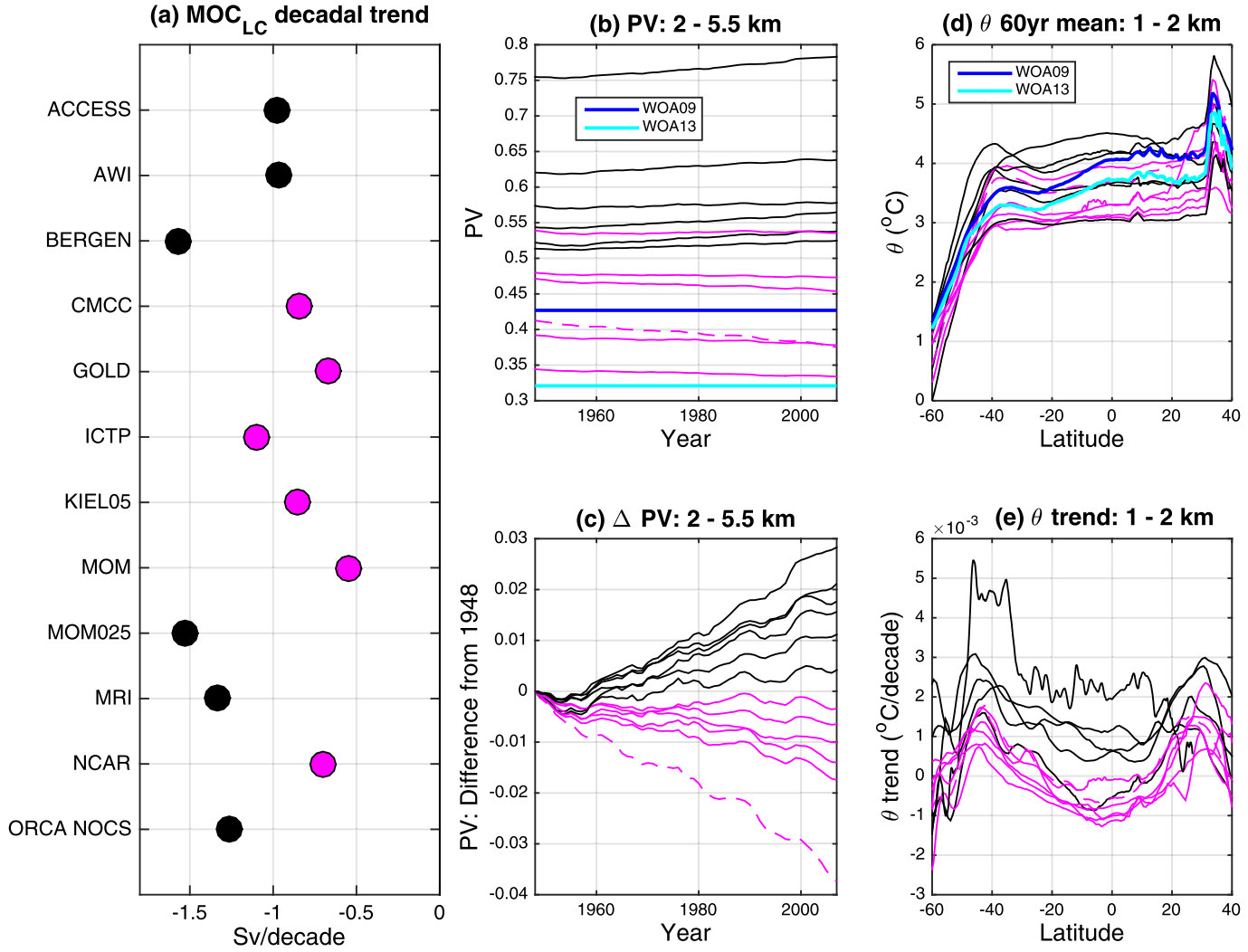

Fig. 5. (a) 60 year trend (Sv/decade) for the decreasing MOC_{LC} in each CORE-II model. Models in black indicate those where the decreasing trend is largest; magenta for smaller decreasing trends. (b) zonal mean potential vorticity (PV; $\times 10^{-11}$ m^{-1} s^{-1}), averaged over the 2 to 5.5 km range for the models indicated by black and magenta in panel a. The observational potential vorticity estimate from the World Ocean Atlas climatology (WOA09/WOA13) is shown by the blue/cyan dashed line. (c) zonal mean potential vorticity averaged over the 2 to 5.5 km range, shown as a difference in the panel b time series from 1948. Negative difference indicates a weakening of stratification; positive indicates strengthening of stratification. (d) 60 year mean zonal mean temperature averaged over the 1–2 km depth range, with WOA09/WO13 observations show in the blue/cyan dashed curve. (e) The decadal trend in zonal mean temperature, calculated over the 60 year CORE-II period. We note that the ICTP model is represented by the dashed magenta curves in panels (b) to (e), as its MOC_{LC} decadal trend is mid-range. (For interpretation of the references to color in this figure legend, the reader is referred to the web version of this article.)

largest equatorward shift in outcropping isopycnals (Fig. 7). This density range also coincides with the latitudinal region where wind stress increases are largest as the westerly the winds intensify and shift polewards over the CORE-II period (Fig. 1b).

In summary, surface heat fluxes influence the intermediate ocean temperature and water column stratification, with differences in surface heat and freshwater fluxes across the models being largest over intermediate and deep water mass ranges where the surface wind stress changes are largest.

4. Summary and discussion

Representation of Southern Ocean large-scale circulation features range widely in multi-model studies, making it difficult to extract key circulation trends and associated mechanisms, such as wind stress and buoyancy fluxes. Here we evaluate key Southern Ocean metrics across a major multi-model effort, namely CORE-II, using the 1948–2007 timeseries. The advantage of using the CORE-II models in this analysis is that their coherent poleward intensification of the westerly winds allows us to somewhat isolate the role of surface buoyancy fluxes and stratification on overturning circulation trends. The poleward intensification of the westerly winds steepens isopycnals in the ACC region, particularly over the region where deep waters upwell. However, surface warming and a large eddy-induced overturning circulation combat this steeper isopycnal gradient. Our main results are summarised as two scenarios in Fig. 8. In brief, the configuration of the eddy parameterisation and the ocean density field are strongly linked with the magnitude of the MOC trends on decadal timescales.

The Fig. 8 upper panel represents models with weak upper stratification, and strong deep stratification in the Southern Ocean. Models that behave in this way generally have a 1D or 2D eddy parameterisation (and thus a smaller MOC_{GM}), associated with larger trends in the MOC_{UC}. However, eddies alone do not account for the stratification patterns over the entire water column. The surface heat fluxes at the junction where deep waters are upwelled in the Southern Ocean and transformed into lighter intermediate waters are associated with the temperature field at intermediate depths in the ocean interior, and this can also alter the ocean stratification. Models with a larger heat-driven

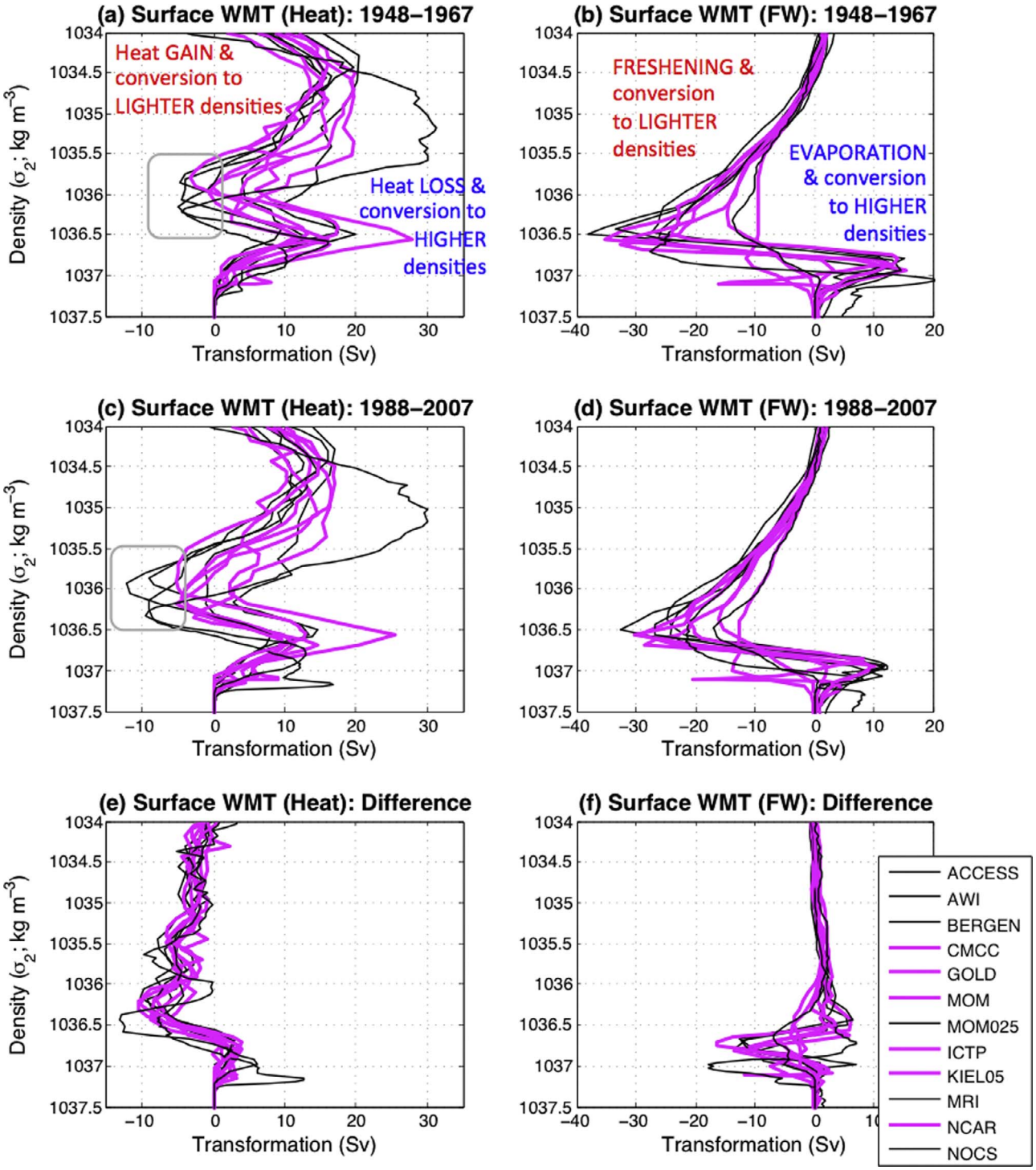

Fig. 6. Surface water mass transformation (WMT; Sv) south of 30°S associated with heat (a, c, e) and freshwater (b, d, f) input, plotted in density coordinates (σ_2; kg m^{-3}), averaged over the 1948–1967 (upper) and 1988–2007 (middle) periods. The last row shows time differences ([1988–2007] minus [1948–1967]) for the surface heat (e) and freshwater (f) WMT. See text for the WMT definition. Positive WMT transports indicate conversion of water masses via surface buoyancy *loss* to *higher* densities, and negative transports indicate conversion of water masses via surface buoyancy *gain* to *lower* densities. Models in black are those shown in Fig. 5 with a larger decreasing MOC_{LC} trend; magenta for those with a smaller decreasing trend. The grey boxes shown around 1035.5–1036.5 kg m^{-3} in panels a and c indicate where the black and magenta contours show a key difference (see text for further details). Note the different *x*-axis scales for the left and right columns. (For interpretation of the references to color in this figure legend, the reader is referred to the web version of this article.)

surface water mass transformation at the deep water/intermediate water junction have a warmer intermediate ocean layer (1 to 2 km). The weak upper ocean stratification enables the poleward intensification of the westerly winds to maximise its influence on increasing the upper overturning circulation. Further, this warmer intermediate layer creates a stronger stratification in the deep ocean below 2 km. Models with a stronger deep ocean stratification exhibit a greater sensitivity of the MOC_{LC} to surface forcing, presumably because the stratification more effectively impedes vertical transport. Four of the models (ACCESS, BERGEN, MRI and NOCS) show both a larger decadal increasing

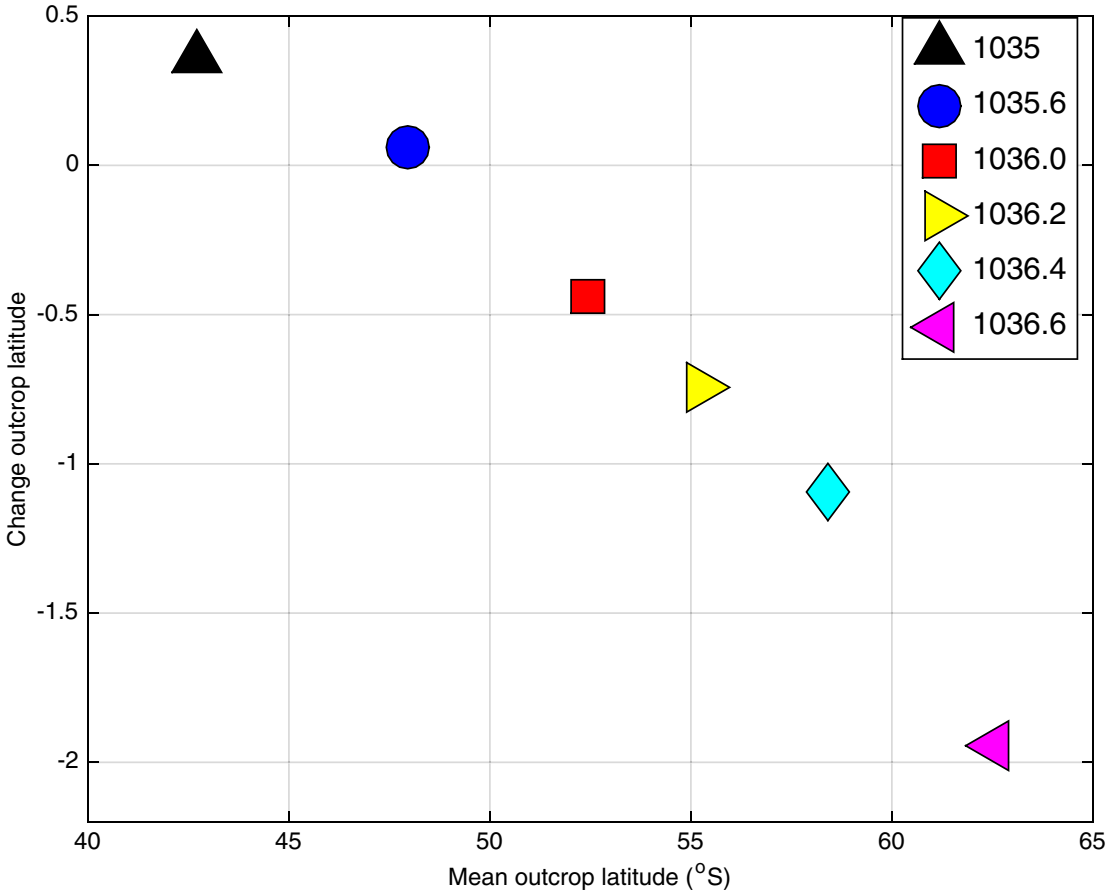

Fig. 7. The final 20 year average density outcrop versus the latitudinal shift in the density outcrop (last minus first 20 year averages). Shown are six isopycnals of interest; units in kg m^{-3}. A positive change in outcrop position along the *y*-axis indicates a *poleward* shift in the outcrop and a reduced surface density locally; a negative change indicates an *equatorward* shift and a local surface densification. The correlations are calculated individually in all twelve models, with the average across the twelve models shown here.

trend in the MOC_{UC} and a larger decadal decreasing trend in the MOC_{LC}.

Conversely, in the alternative scenario (Fig. 8; lower panel), models with weak heat-driven surface transformation and a cooler intermediate ocean layer in the mean state exhibit a *smaller* decadal decreasing trend in the MOC_{LC}. In the upper ocean, a stronger stratification and a more complex 3D eddy parameterisation (i.e., a larger MOC_{GM}) are associated with smaller increases in the MOC_{UC} on decadal timescales. Four of the six models (CMCC, GOLD, KIEL05 and NCAR) with a weaker decreasing MOC_{LC} trend also show a weaker MOC_{UC} trend. We note that improving the configuration of eddy parameterisation alone does not produce a more realistic ocean stratification. However, the lower panel of Fig. 8 does contain both a larger eddy contribution to the upper MOC and a weaker deep ocean stratification that is more aligned with observations (see Fig. 5), compared to the upper panel scenario.

This study offers new insights into how large scale MOC metrics are linked to eddies and stratification in a multi-model analyses, but there are, of course, caveats. Firstly, we are assessing metrics from a zonal mean perspective, however oceanic and atmospheric features are zonally asymmetric and this regional variation is not taken into account here. Though we note that those conducting large-scale multi-model analyses usually have neither the time or model output storage capabilities to produce analyses that compares extensive regional detail across multiple models. Further, we have focused here on metrics influencing the overturning circulation that are readily discussed and published, making our results easily testable in future model simulations. The 300-year CORE-II period is too short for the deep ocean to reach a thermodynamic equilibrium, and thus we expect minor deep ocean drift in the final cycle analysed. However, Farneti et al. (2015) has shown that large-scale Southern Ocean circulation trends are persistent within each 60-year cycle.

Here we analyse twelve models coupled to a common atmospheric state, whereas other recent multi-model efforts, such as CMIP5, have fully-coupled climate model contributions. In these types of models, there is a two way flux of ocean and atmosphere variables, that is, the ocean can influence the atmospheric state. Further, fully coupled model comparisons have revealed a large spread in wind stress position and strength, making it near impossible to isolate the influence of wind stress versus buoyancy fluxes in an evolving climate. Whether our results hold in a fully-coupled multi-model comparison is yet to be tested, particularly due to the shortage of CMIP5 models that archive the overturning circulation in density space. Nonetheless, using a multi-model effort with a common (but varying) atmospheric state, such as CORE-II, allows for some control over how many variables and model components change over time.

The main conclusion of this study is that model biases in the mean and varying states of temperature, salinity, surface buoyancy fluxes, and configuration of the eddy parameterisation in coarse resolution models influence the sensitivity of the upper and lower overturning circulation cells. Our results are not impacted by the spread of MOC transports in the mean state, nor the model vertical grid resolution. For future multi-model efforts, we suggest that the temporal evolution of the eddy circulation, surface buoyancy fluxes, and interior ocean

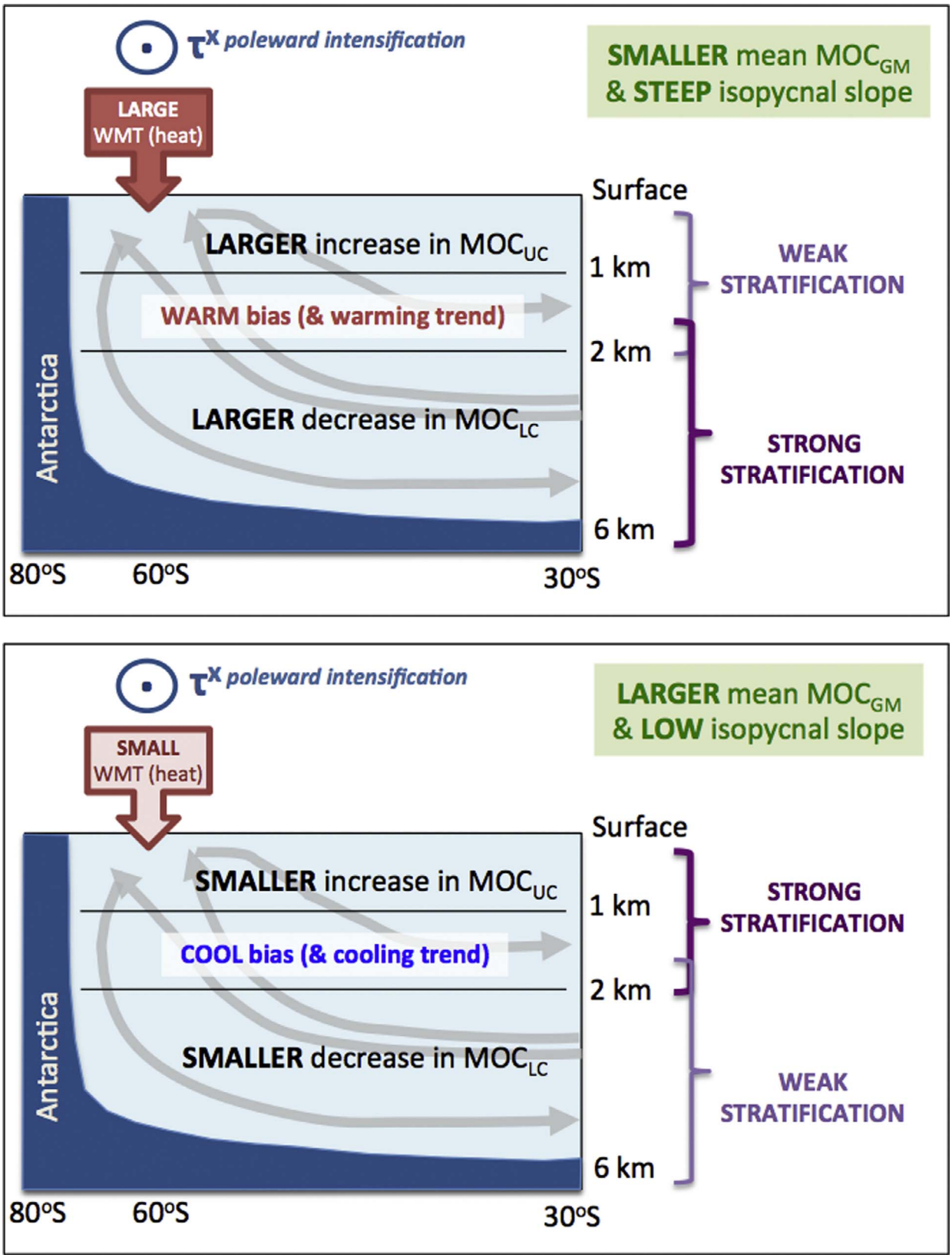

Fig. 8. Summary schematic of how surface heat fluxes and stratification influence the magnitude of the decadal trends in the Southern Ocean overturning circulation. Illustrated are the surface heat water mass transformation (WMT), zonal wind stress (τ^x) that shifts poleward and intensifies over the CORE-II period, the upper and lower meridional overturning circulation (MOC_{UC} and MOC_{LC}), ocean stratification, and temperature. In the upper panel, the eddy-induced overturning circulation is smaller, associated with steeper isopycnals within the Antarctic Circumpolar Current region. See text for full description.

density biases be a key focus as a mechanism for overturning circulation changes.

Acknowledgments

The authors wish to thank R. Farneti for assistance with model output, O. Saenko for eddy coefficients in the CanESM2 model, and M. Nikurashin for discussions on overturning circulation and wind stress. We are grateful for the constructive comments provided by three anonymous reviewers. SMD was supported by the Australian Governments Business Cooperative Research Centres Programme through the Antarctic Climate and Ecosystems Cooperative Research Centre (ACE CRC) and PS by an Australian Research CouncilDECRA Fellowship DE150100223.

References

Antonov, J., Seidov, D., Boyer, T.P., Locarnini, R.A., Mishonov, A.V., Garcia, H.E., Baranova, O.K., Zweng, M.M., Johnson, D.R., 2010. Volume 2: Salinity. In: Levitus, S. (Ed.), World Ocean Atlas 2013. NOAA Atlas NESDIS 69, pp. 184.

Armour, K.C., Marshall, J., Scott, J.R., Donohoe, A., Newsom, E.R., 2016. Southern Ocean warming delayed by circumpolar upwelling and equatorward transport. Nat. Geosci. 9, 549–554.

Boning, C.W., Dispert, A., Visbeck, M., Rintoul, S.R., Schwarzkopf, F.U., 2008. The response of the antarctic circumpolar current to recent climate change. Nat. Geosci. 1 (12), 864–869.

Chapman, C., Sallée, J.-B., 2017Chapman, Sallée. Isopycnal mixing suppression by the Antarctic Circumpolar Current and the Southern ocean Meridional Overturning Circulation. J. Phys. Oceanogr. 47 (8), 2023–2045.

Chidichimo, M.P., Donohue, K.A., Watts, D.R., Tracey, K.L., 2014. Baroclinic transport time series of the antarctic circumpolar current measured in drake passage. J. Phys. Oceanogr. 44 (7), 1829–1853. http://dx.doi.org/10.1175/JPO-D-13-071.1.

Cunningham, S.A., Alderson, S.G., King, B.A., Brandon, M.A., 2003. Transport and variability of the Antarctic Circumpolar Current in Drake Passage. J. Geophys. Res. 108 (C5). doi:10.1029/2001JC001147.

Danabasoglu, G., Yeager, S.G., Bailey, D., Behrens, E., Bentsen, M., Bi, D., Biastoch, A., Bning, C., Bozec, A., Canuto, V.M., Cassou, C., Chassignet, E., Coward, A.C., Danilov, S., Diansky, N., Drange, H., Farneti, R., Fernandez, E., Fogli, P.G., Forget, G., Fujii, Y., Griffies, S.M., Gusev, A., Heimbach, P., Howard, A., Jung, T., Kelley, M., Large, W.G., Leboissetier, A., Lu, J., Madec, G., Marsland, S.J., Masina, S., Navarra, A., Nurser, A.G., Pirani, A., y Mlia, D.S., Samuels, B.L., Scheinert, M., Sidorenko, D., Treguier, A.-M., Tsujino, H., Uotila, P., Valcke, S., Voldoire, A., Wang, Q., 2014. North Atlantic simulations in Coordinated Ocean-ice Reference Experiments Phase II (CORE-II). Part I: Mean states. Ocn.Modell. 73 (0), 76–107. http://dx.doi.org/10.1016/j.ocemod.2013.10.005.

Donohue, K.A., Tracey, K.L., Watts, D.R., Chidichimo, M.P., Chereskin, T.K., 2016. Mean Antarctic Circumpolar Current transport measured in Drake Passage. Geophys. Res. Lett. 43 (22), 11,760–11,767. http://dx.doi.org/10.1002/2016GL070319.

Döös, K., Webb, D.J., 1994. The Deacon Cell and other meridional cells of the Southern Ocean. J. Phys. Oceanogr. 24, 429–442.

Downes, S.M., Farneti, R., Uotila, P., Griffies, S.M., Marsland, S.J., Bailey, D., Behrens, E., Bentsen, M., Bi, D., Biastoch, A., Böning, C., Bozec, A., Canuto, V.M., Chassignet, E., Danabasoglu, G., Danilov, S., Diansky, N., Drange, H., Fogli, P.G., Gusev, A., Howard, A., Ilicak, M., Jung, T., Kelley, M., Large, W.G., Leboissetier, A., Long, M., Lu, J., Masina, S., Mishra, A., Navarra, A., Nurser, A.G., Patara, L., Samuels, B.L., Sidorenko, D., Spence, P., Tsujino, H., Wang, Q., Yeager, S.G., 2015. An assessment of southern ocean water masses and sea ice during 1988–2007 in a suite of interannual core-ii simulations. Ocean Model. 94, 67–94. https://doi.org/10.1016/j.ocemod.2015.07.022.

Downes, S.M., Gnanadesikan, A., Griffies, S.M., Sarmiento, J.L., 2011. Water mass exchange in the Southern Ocean in coupled climate models. J. Phys. Oceanogr. 41, 1756–1771.

Downes, S.M., Hogg, A.M., 2013. Southern ocean circulation and eddy compensation in CMIP5 models. J. Clim. 26 (18), 7198–7220. http://dx.doi.org/10.1175/JCLI-D-12-00504.1.

Farneti, R., Delworth, T.L., Rosati, A.J., Griffies, S.M., Zeng, F., 2010. The role of mesoscale eddies in the rectification of the southern ocean response to climate change. J. Phys. Oceanogr. 40 (7), 1539–1557. http://dx.doi.org/10.1175/2010JPO4353.1.

Farneti, R., Downes, S.M., Griffies, S.M., Marsland, S.J., Behrens, E., Bentsen, M., Bi, D., Biastoch, A., Böning, C., Bozec, A., Canuto, V.M., Chassignet, E., Danabasoglu, G., Danilov, S., Diansky, N., Drange, H., Fogli, P.G., Gusev, A., Hallberg, R.W., Howard, A., Ilicak, M., Jung, T., Kelley, M., Large, W.G., Leboissetier, A., Long, M., Lu, J., Masina, S., Mishra, A., Navarra, A., Nurser, A.G., Patara, L., Samuels, B.L., Sidorenko, D., Tsujino, H., Uotila, P., Wang, Q., Yeager, S.G., 2015. An assessment of antarctic circumpolar current and southern ocean meridional overturning circulation during 1958–2007 in a suite of interannual core-ii simulations. Ocean Model. 93, 84–120. https://doi.org/10.1016/j.ocemod.2015.07.009.

Gent, P.R., 2016. Effects of Southern Hemisphere wind changes on the meridional overturning circulation in ocean models. Ann. Rev. Mar. Sci. 8, 79–94. http://dx.doi.org/10.1146/annurev-marine-122414-033929.

Gent, P.R., Danabasoglu, G., 2011. Response to increasing southern hemisphere winds in CCSM4. J. Clim. 24 (19), 4992–4998. http://dx.doi.org/10.1175/JCLI-D-10-05011.1.

Gent, P.R., McWilliams, J.C., 1990. Isopycnal mixing in ocean circulation models. J. Phys. Oceanogr. 20, 150–155.

Gleckler, P.J., Taylor, K.E., Doutriaux, C., 2008. Performance metrics for climate models. J. Geophys. Res. 113 (D06104). http://dx.doi.org/10.1029/2007JD008972.

Heuzé, C., Heywood, K.J., Stevens, D.P., Ridley, J.K., 2013. Southern ocean bottom water characteristics in cmip5 models. Geophys. Res. Lett. 40 (7), 1409–1414. http://dx.doi.org/10.1002/grl.50287.

Hogg, A.M., Spence, P., Saenko, O., Downes, S.M., 2017. The energetics of Southern Ocean upwelling. J. Phys. Oceanogr. 47, 135–153. http://dx.doi.org/10.1175/JPO-D-16-0176.1.

Large, W., Yeager, S.G., 2009. The global climatology of an interannually varying air-sea flux data set. Clim. Dyn. 33 (5682), 341–364. http://dx.doi.org/10.1007/s00382-008-0441-3.

Locarnini, R.A., Mishonov, A.V., Antonov, J.I., Boyer, T.P., Garcia, H.E., Baranova, O.K., Zweng, M.M., Johnson, D.R., 2010. Volume 1: temperature. In: Levitus, S. (Ed.), World Ocean Atlas 2013. NOAA Atlas NESDIS 68, pp. 184pp.

Locarnini, R.A., Mishonov, A.V., Antonov, J.I., Boyer, T.P., Garcia, H.E., Baranova, O.K., Zweng, M.M., Paver, C.R., Reagan, J.R., Johnson, D.R., Hamilton, M., Seidov, D., 2013. Volume 1: Temperature. In: Levitus, S., Mishonov, A. (Eds.), World Ocean Atlas 2013. NOAA Atlas NESDIS 73, pp. 40pp.

Lumpkin, R., Speer, K., 2007. Global ocean meridional overturning. J. Phys. Oceanogr. 37 (10), 2550–2562. http://dx.doi.org/10.1175/JPO3130.1.

Mahlstein, I., Gent, P.R., Solomon, S., 2013. Historical antarctic mean sea ice area, sea ice trends, and winds in CMIP5 simulations. J. Geophys. Res.: Atmos. 118 (11), 5105–5110. http://dx.doi.org/10.1002/jgrd.50443.

Marshall, J., Scott, J.R., Romanou, A., Kelley, M., Leboissetier, A., 2017. The dependence of the ocean's MOC on mesoscale eddy diffusivities: a model study. Ocn. Model. 111, 1–8. doi:i0.1016/j.ocemod.2017.01.001.

Meijers, A.J.S., Shuckburgh, E., Bruneau, N., Sallee, J.-B., Bracegirdle, T.J., Wang, Z., 2012. Representation of the antarctic circumpolar current in the CMIP5 climate models and future changes under warming scenarios. J. Geophys. Res.: Oceans 117 (C12). C12008. doi:10.1029/2012JC008412.

Morrison, A.K., Hogg, A.M., 2013. On the relationship between Southern Ocean overturning and ACC transport. J. Phys. Oceanogr. 43 (1), 140–148. http://dx.doi.org/10.1175/JPO-D-12-057.1.

Purkey, S.G., Johnson, G.C., 2012. Global contraction of Antarctic Bottom Water between the 1980s and 2000s. J. Clim. 25, 5830–5844. http://dx.doi.org/10.1175/JCLI-D-11-00612.1.

Rintoul, S., Naveira Garabato, A.C., 2013. Dynamics of the Southern Ocean Circulation – Chapter 18. In: Siedler, G., Griffies, S., Church, J., Gould, J. (Eds.), In: Ocean Circulation and Climate, 2nd Edition. 103 International Geophysical Series, Academic Press.

Russell, J.L., Stouffer, R.J., Dixon, K.W., 2006. Intercomparison of the southern ocean circulations in ipcc coupled model control simulations. J. Clim. 19 (18), 4560–4575. http://dx.doi.org/10.1175/JCLI3869.1.

Saenko, O.A., sen Gupta, A., Spence, P., 2012. On challenges in predicting bottom water transport in the Southern Ocean. J. Phys. Oceanogr. 25, 1349–1356. J. Clim. doi:10.1175/JCLI-D-11-00040.1.

Shu, Q., Song, Z., Qiao, F., 2015. Assessment of sea ice simulations in the CMIP5 models. Cryosphere 9 (1), 399–409. http://dx.doi.org/10.5194/tc-9-399-2015.

Sijp, W.P., England, M.H., 2009. Southern hemisphere westerly wind control over the ocean's thermohaline circulation. J. Clim. 22 (5), 1277–1286. http://dx.doi.org/10.1175/2008JCLI2310.1.

Speer, K., Guilyardi, E., Madec, G., 2000. Southern Ocean transformation in a coupled model with and without eddy mass fluxes. Tellus 52A, 554–565.

Spence, P., van Sebille, E., Saenko, O., England, M., 2014. Using Eulerian and Lagrangian approaches to investigate wind-driven changes in the Southern Ocean abyssal circulation. J. Phys. Oceanogr. 44, 662–675.

Talley, L.D., 2013. Closure of the global overturning circulation through the Indian, Pacific, and Southern Oceans: Schematics and transports. Oceanography 26 (1), 80–97.

Walin, G., 1982. On the relation between sea-surface heat flow and thermal circulation in the ocean. Tellus 34 (2), 187–195. http://dx.doi.org/10.1111/j.2153-3490.1982.tb01806.x.

Wang, Z., Kuhlbrodt, T., Meredith, M.P., 2011. On the response of the antarctic circumpolar current transport to climate change in coupled climate models. J. Geophys. Res.: Oceans 116 (C8). C08011. doi:10.1029/2010JC006757.

Zweng, M., Reagan, J., Antonov, J., Locarnini, R., Mishonov, A., Boyer, T., Garcia, H., Baranova, O., Johnson, D., D.Seidov, M.B., 2013. Volume 2: Salinity. In: Levitus, S., Mishonov, A. (Eds.), World Ocean Atlas 2013. NOAA Atlas NESDIS 74, pp. 39pp.